The Geographical Journal of Nepal
Vol. 19: 23-43, 2026
DOI: https://doi.org/10.3126/gjn.v19i1.92144
Central Department of Geography,
Tribhuvan University, Kathmandu, Nepal

Flood Hazard Mapping and Risk Evaluation in the Lower Karnali River Basin of Nepal

Laxmi Chhinal[1], Sudeep Thakuri[2]*, Ajay Bhakta Mathema[1], Bipin Dulal[3], Sanjay Nath Khanal[1]

[1]School of Environmental Science and Management, Pokhara University, Kathmandu, Nepal

[2]Central Department of Environmental Science, Tribhuvan University, Kathmandu, Nepal

[3]Hamburg University of Technology TUHH, Humburg, Germany

*Corresponding email: sudeep.thakuri@cdes.tu.edu.np

Received: 20 December, 2025; Accepted: 17 January, 2026; Published: March, 2026

Abstract

This study presents flood hazard mapping and risk assessment using a hydrodynamic simulation in HEC-RAS tool, focusing on a 38 km stretch of the river from Chisapani to the Nepal-India border in the Lower Karnali River Basin (KRB). A time series of daily mean discharge records from the Chisapani gauging station was used for model simulations. Flood magnitudes of 10-, 20-, 50-, and 100- year return periods (YRPs) were estimated using Gumbel's distribution, with the 100-YRP daily discharge of 20,343 m^3/s. Field surveys were conducted in flood-prone areas of Rajapur Municipality using the Vulnerability and Risk Assessment (VRA) framework. Results show that parts of Rajapur Municipality, Wards #1, #3, #4, and #7 are susceptible to inundation, even during normal flood events, with water depths reaching upto 10 m posing significant risk to the communities inhabiting in these areas. Agricultural land is particularly exposed, posing serious risks to food security and livelihoods. Moreover, even after a five-year return period, the 2014 flood simulations (equal to a 100-YRP) indicate that these wards remains highly vulnerable. This findings emphasizes the urgent need for improved settlement planning and the development of effective flood control measures in Rajpur Municipality.

Keywords: *hazard mapping, risk, discharge, return period, HEC-RAS.*

Introduction

Floods pose a great threat to human livelihoods and global development (Rentschler *et al.,* 2022). Projections indicate that population growth and the expansion of economic assets in flood-prone regions could triple flood exposure by 2050 (Jongman *et al.,* 2012). Flood risk is particularly acute in South Asia and the Pacific, where 668 million people representing 28% of the region's total population are exposed. Globally, approximately 1.81 billion people live in flood-vulnerable areas (Rentschler *et al.,* 2022). In Nepal, flooding ranks among the most devastating water-induced hazards, threatening lives, infrastructure, and livelihoods. This risk is further exacerbated by increasing population pressures, the expansion of settlements, including informal squatter communities, along riverbanks, and the intensifying impacts of climate change (Maranzoni *et al.,* 2023; Dangol & Bormudoi, 2015).

Nepal is already experiencing the consequences of climate change. Shifts in weather patterns, an increase in the frequency of extreme weather events, and irregular seasonal behaviour have rendered traditional and indigenous knowledge less reliable (Felkner *et al.,* 2009). Between 1976 and 2015, Nepal recorded an average annual increase in maximum temperature of +0.045°C/year, indicating a clear warming trend (Thakuri *et al.,* 2019).

Monsoon rainfall has become increasingly erratic and intense due to climate-induced changes in the hydrological cycle, driven largely by rising greenhouse gas emissions from deforestation, urbanization, and industrialization (Poornima *et al.,* 2024; IPCC, 2019; Hisdal *et al.,* 2001). These changes have led to more frequent and severe flash floods and riverine floods, which disproportionately affect poor and marginalized populations by damaging critical infrastructure, disrupting food and water systems, and threatening human well-being. In this context, vulnerability refers to the degree of potential loss or harm that such hazards may cause to exposed individuals, infrastructure, and systems (Rusk *et al.,* 2022; MoPE, 2017).

The southern lowlands of Nepal, the Terai region, are particularly prone to flooding during the summer monsoon months (June–August). Rivers rise sharply during intense rainfall events, often overflowing their banks and inundating large areas. The frequency and severity of such floods have increased over recent decades. Flood conditions are further exacerbated by infrastructure such as embankments and barrages constructed across the border in India, which impede natural drainage and contribute to annual waterlogging and inundation in border communities, intensifying flood impacts (Dangol, 2020).

The Karnali River, in particular, is known for its recurrent and severe floods. Originating between the Dhaulagiri and Nanda Devi ranges in western Nepal, the Karnali River

Basin (KRB) spans approximately 45,269 km² (Khatiwada *et al.,* 2016), with an average annual discharge of 1,441 m³/s. Notable flood events have occurred in 1963, 1983, 2008, 2013, and 2014, with the 2014 flood breaching danger levels and inundating downstream communities, causing widespread damage and displacement. Such events highlight the persistent vulnerability of these regions to flooding, with similar patterns recurring over time (Venkateswaran *et al.,* 2015).

Previous studies have predominantly neglected integrated, high-resolution hydrodynamic models calibrated specifically for flood-vulnerable sub-basins, including the Lower KRB, a region in Nepal frequently affected by flooding that displaces thousands of people each year and damages infrastructure. Comprehensive risk assessments that combine hydraulic simulations with local infrastructure, land-use, and demographic data remain limited. Many existing studies depend on coarse-resolution global models that cannot accurately represent sub-basin dynamics (Winsemius *et al.,* 2013). In addition, the lack of evidence-based tools for community-level adaptation planning limits effective mitigation in the face of increasing climate variability and socioeconomic pressures.

This study addresses these gaps by applying a hydrodynamic modeling approach for the lower KRB. It combines high-resolution flood simulations for multiple return periods with geospatial analyses of infrastructure, land use, and population data to produce practical flood risk maps and adaptation strategies. Focusing on frequently flooded areas such as Rajapur, the approach supports proactive river management, reduces socioeconomic impacts, strengthens community resilience, improves settlement planning, and guides effective flood mitigation measures.

Methodology

Study Area

This study examines the lower KRB in Nepal (2,025 km²; Figure 1), targeting the stretch from upstream Chisapani to downstream Rajapur Municipality (Wards #1, #3, #4, and #7) in Bardiya District, Lumbini Province among the basin's most flood-prone areas due to their adjacency to the Karnali River and its distributaries (Pokhrel *et al.,* 2021). The subtropical monsoon climate delivers 80-90% of annual rainfall during June-September, plus pre-monsoon surges (April-May), fueling recurrent inundation. Land use/land cover (LULC) is dominated by agricultural plains, northern forests, and delta wetlands, with exposed croplands and settlements in Rajapur. The 2021 census reports 61,431 residents (32,265 female, 29,166 male), primarily Tharu communities reliant on subsistence agriculture, heightening vulnerability to flood damages in livelihoods, food security, property, and infrastructure.

Figure 1

Location of Study Area: the Lower Karnali River Basin (KRB) of Nepal. The Map also Shows Different Wards of the Rajapur Municipality of Bardia District, Nestled in Lower KRB

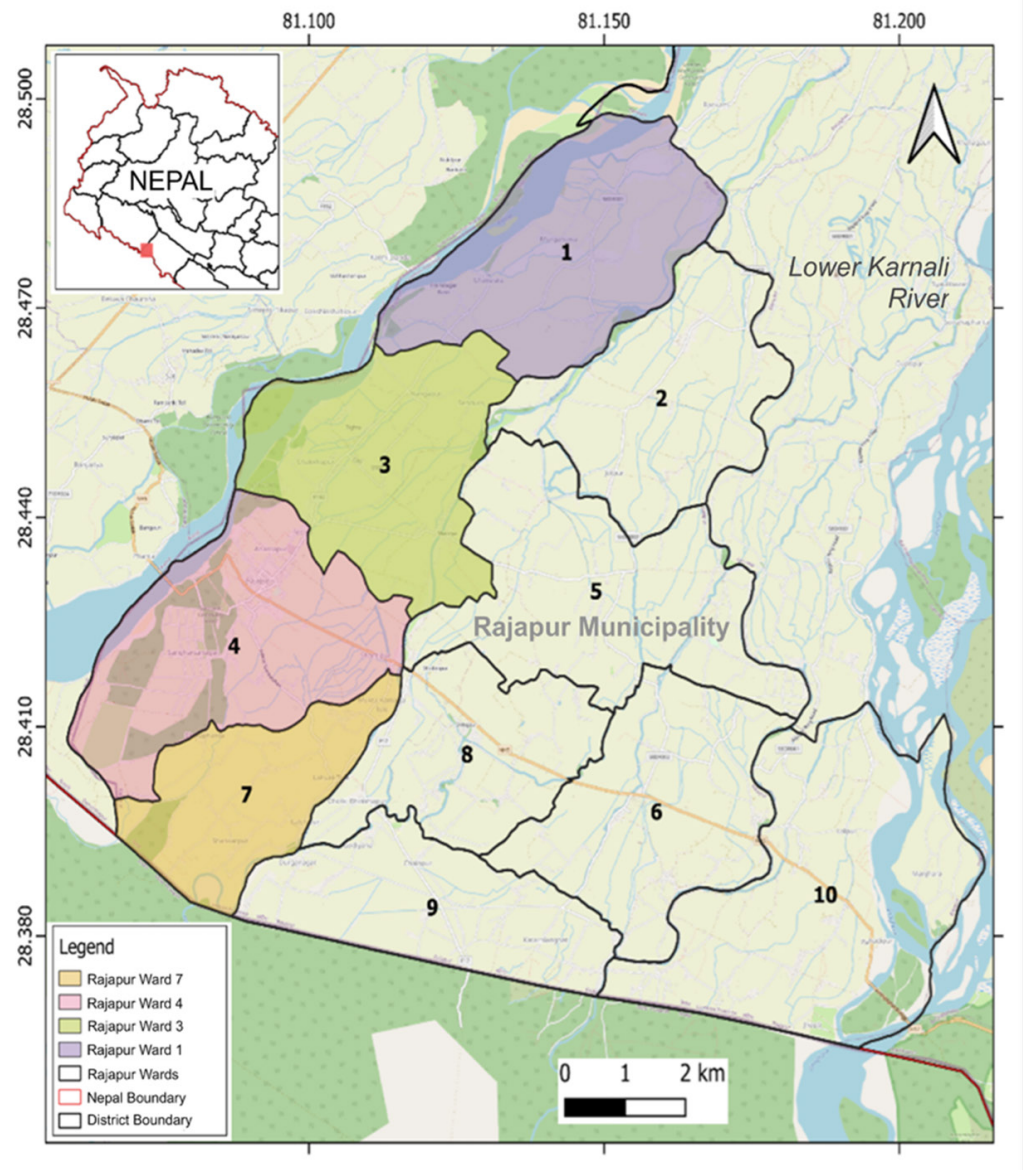

Data and Methods

Figure 2 presents the conceptual framework of the study, linking the research objectives to the methods.

Figure 2

Conceptual Framework of the Study

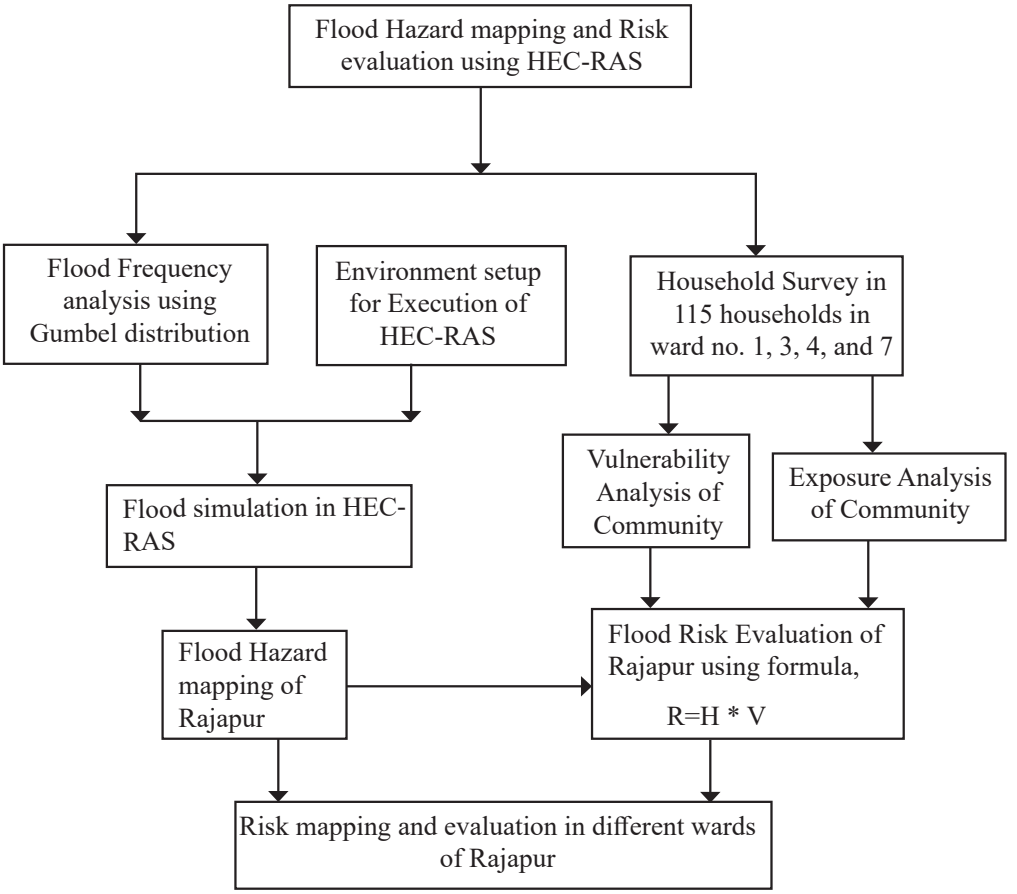

Data Source

The data source for this study includes household surveys, key informant interviews (KIIs), focus group discussions (FGDs), and global positioning system (GPS) mapping in the field. Furthermore, hydrological records. high-resolution Digital Elevation Models (DEM), river cross-section profiles, land use maps, municipal household records are collected from different sources for flood modeling, terrain analysis, and spatial mapping of hazard zones.

Field Survey: Field data collection targeted residents and local stakeholders in flood-prone settlements to obtain detailed, locally relevant information. A total of 120 households were surveyed across four wards using stratified random sampling to ensure representation across different exposure levels.

The sample size was designed to ensure statistical validity (Kwak & Kim, 2017). Survey questionnaires captured information on household income dependency, infrastructure condition, access to early warning systems, settlement characteristics, and coping strategies. KIIs and FGDs were conducted to complement household data with institutional and community perspectives. The integration of community-level insights with hydrological and spatial datasets enabled a comprehensive understanding of flood risk in the lower KRB. Data were collected using the KOBO Toolbox to enhance accuracy and efficiency.

Hydrological and Spatial Data: Hydrological data consisting of 30 years (1991–2021) of discharge records were obtained from the Department of Hydrology and Meteorology (DHM), Chisapani station, to analyze long-term flow trends and support hydraulic modeling.

For flood hazard mapping, a 5 m resolution ALOS World 3D DEM was used. Land-use maps were obtained from the International Centre for Integrated Mountain Development (ICIMOD).

River cross-sections were generated and analyzed using HEC-RAS to simulate flood scenarios and delineate inundation areas. Additional supporting information was gathered from relevant secondary sources and published literature.

Vulnerability Assessment

This study adopts the Vulnerability and Risk Assessment (VRA) framework outlined by MoPE (2017), which quantifies vulnerability through composite indicators across biophysical, socioeconomic, and institutional dimensions. Vulnerability (V) was calculated using the normalized index (MoPE, 2017; IPCC, 2014),

$$V = \frac{Exposure \times Sensitivity}{Adaptive\,Capacity} \quad (1)$$

Each component was derived from field survey data (household surveys, FGDs, and KIIs) and census demographics and land-use records.

Contributing factors (CFs) and associated indicators such as household income dependency on agriculture, infrastructure quality, access to early warning systems,

and settlement density were collected via structured household surveys. The indicators were organized in Excel and normalized using min-max scaling (0-1 range) prior to aggregation into the composite vulnerability index (MoPE, 2017).

Table 1

Indicators of Exposure, Sensitivity and Adaptive Capacity for Vulnerability Assessment

Exposure	Sensitivity	Adaptive capacity
– No. of people involve in Agriculture	– Nature of house	– Education of household head
– Distance from river	– Source of income	– Types of embankments
– Exposed agricultural land	– Population Distribution	– Access to early warning
– Land use type near household	– Types of flood tolerance crops	– No. of flood trained member of family.
	– Types of Settlement	– No. of cattle in house

The indicators values were normalized as an index (value ranging from 0 to 1), using the min-max method (Vashishtha & Fazal, 2025):

$$Index_i = \frac{x - x_{min}}{x_{max} - x_{min}} \quad (2)$$

where, X = Original value, Xmin = Minimum value in the dataset, Xmax = Maximum value in the dataset, $Index_i$ = Normalized value of indicator i.

An equal weight (Žurovec *et al.,* 2017) was assigned to all components and averaged using the eq (2) .

$$C_J = \frac{\sum_{i-1}^{nj} Index_i}{n_j} \quad (3)$$

where, n_j = no. of indicators under component j, $Index_i$ = normalized value of sup-indicators, C_j = Score of component j (exposure, sensitivity and adaptive capacity).

Finally, the vulnerability of each ward was computed by,

Vulnerability = (Exposure + Sensitivity) - Adaptive Capacity (4)

Flood Mapping

Watershed Delineation and Catchment Area Calculation: For flood hazard mapping, watershed boundary and river networks for the area was derived from the DEM in GIS environment (Figure 3).

Hydrological Analysis: Comparative maximum annual flood discharge for different return periods (10, 20, 50, and 100 yr) was calculated using Gumbel's distribution method (Zelenhasic, 1970). The daily average discharge data of 30 years (1991–2021) was collected from the Chispani gauge station.

Figure 3

Process of Flood Hazard Mapping

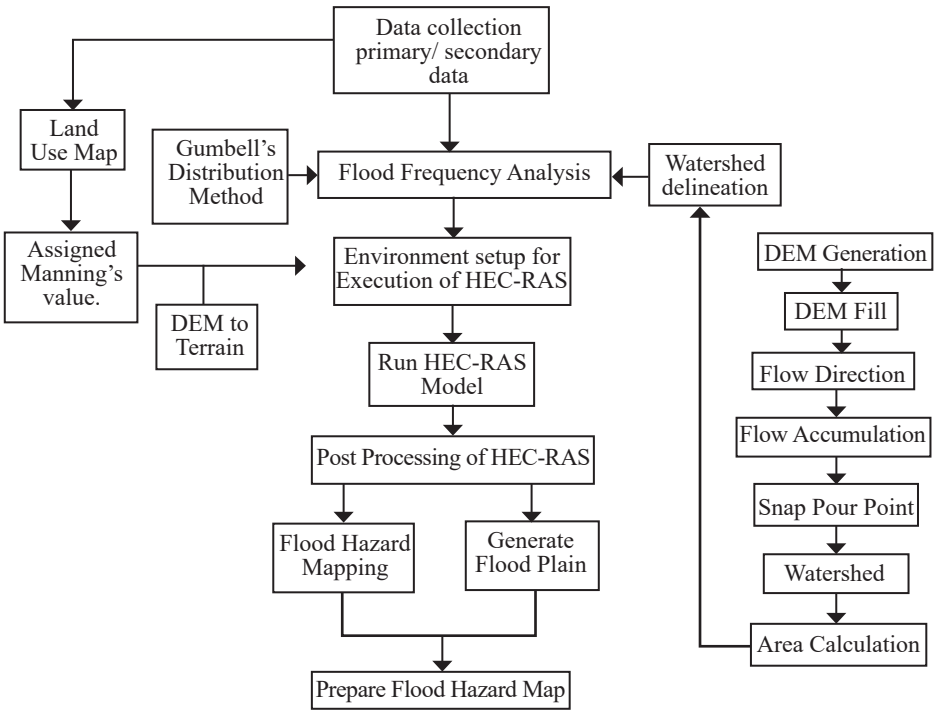

Selection of Model Tools: This study used HEC-RAS version 6.2, developed by the U.S. Army Corps of Engineers (USACE), to simulate water surface profiles and floodplain inundation (Figure 3). QGIS version 3.22.9 was used for geospatial data processing, including terrain analysis, raster reprojection, and risk map generation. HEC-RAS and QGIS were used for hydraulic and spatial analyses (Mohammed *et al*., 2018; Chyon *et al.,* 2023). HEC-RAS enables accurate one- and two-dimensional unsteady flow

simulations for complex river systems (Singh *et al*., 2020), while QGIS supports the integration of hydraulic outputs with socioeconomic data for vulnerability mapping (Regmi *et al.,* 2023; Steiniger & Hunter, 2013).

HEC-RAS Application: A two-dimensional (2D) unsteady flow HEC-RAS model was used to simulate water surface elevations, flow depths, velocities, and inundation extends for 10-, 20-, 50-, and 100-YRP. Thirty years of peak annual discharge data from the upstream Chisapani gauging station were subjected to frequency analysis using the Gumbel distribution to generate inflow hydrographs as upstream boundary conditions. Stage–time rating curves derived from surveyed data were applied as downstream boundary conditions, while dry terrain was assumed as the initial condition. QGIS was used for pre- and post-processing. The DEM was processed in QGIS to derive terrain and hydrological features. Administrative shapefiles for Bardiya District, Rajapur Municipality, and its wards were clipped to the model domain. LULC data (2009 and 2014) at 30-m resolution were obtained from ICIMOD and used to assign Manning's roughness coefficients following HEC-RAS guidelines. Surveyed cross-sections were incorporated to improve model accuracy (Mudashiru *et al.,* 2021).

Table 2

Manning Roughness Coefficients for Different Land Use

LULC ID	Land cover	Manning's n value
1	Waterbodies	0.025
2	Forest	0.16
3	River bed	0.035
4	Built-up	0.15
5	Crop land	0.05
6	Grass land	0.05
7	Forest	0.16

The 2D computational mesh was a structured orthogonal grid with 10 m × 10 m cell sizes (~50,000 cells over the 5-km² domain), inc[orporating the terrain surface, streamlines as breaklines for flow guidance, and LULC-based roughness; simulations used the diffusion wave solver with a 1-second computation interval, calibrated against historical flood data for accuracy (Vashist & Singh, 2023).

Model Calibration and Validation: The hydraulic simulations included model calibration and validation. To ensure satisfactory performance in subsequent simulations, data from two ground stations were used. The model was calobrated and validated using

observed peak discharge and water level data from Chisapani and Satighat stations (Aryal *et al.,* 2020).

Table 3

Instantaneous Peak Discharge and Water Depth at Chisapani and Satighat Hydrological Station (Aryal et al., 2020)

Year	Peak discharge (m^3/s)	Depth (m)
A. Chisapani Hydrological Station		
1983	21,700	15.0
2014	21,700	15.2
1975	16,000	13.0
2009	17,000	13.4
B. *Satighat Station*		
2009	17,000	2.3
2013	-	2.4
2014	21,700	2.6

Figure 4

Comparison Between Observed and Simulated Water Levels at Chisapani and Satighat in River Channel for Flood Events of (a) 2009 and (b) 2014

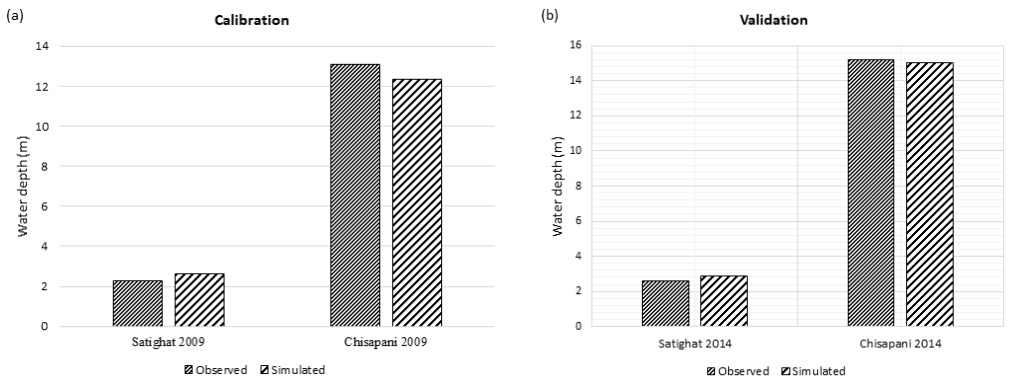

Model performance was assessed by comparing simulated and observed water levels (Hicks & Peacock, 2005). A lower percentage error between the simulated and observed water level indicates a better performance of the model. The simulated 2014 flood water level was with a difference of only 1.3% between the observed (15.2 m) and simulated (15 m) water levels. A detailed comparison of the calibration and validation processes are illustrated in Figure 4.

Results and Discussion

Flood Frequency

Flood frequencies for different YRPs using the log chart along with the recorded historical peak discharges are presented in Table 4 and Figure 5. Among the three types of extreme value distributions, the Type I (Gumbel) distribution was found to be the most appropriate. The discharges predicted by Gumbel's distribution were 13,321, 15,472, 18,256, and 20,343 m^3/s for the 10-, 20-, 50- and 100-YRPs, respectively.

Table 4

Flood Frequency of Different YRP using Gumbel's Distribution Method

SN	Return period (T) in years	Gumbel's value (Q) m^3/s	G_{max}	G_{min}
1	10	13320.39	16139.28	10501.5
2	20	15471.51	19062.14	11880.87
3	50	18255.91	22863.64	13648.18
4	100	20342.43	25719.36	14965.51

Figure 5

Frequency Analysis of Flood Discharge at Chisapani Gauge

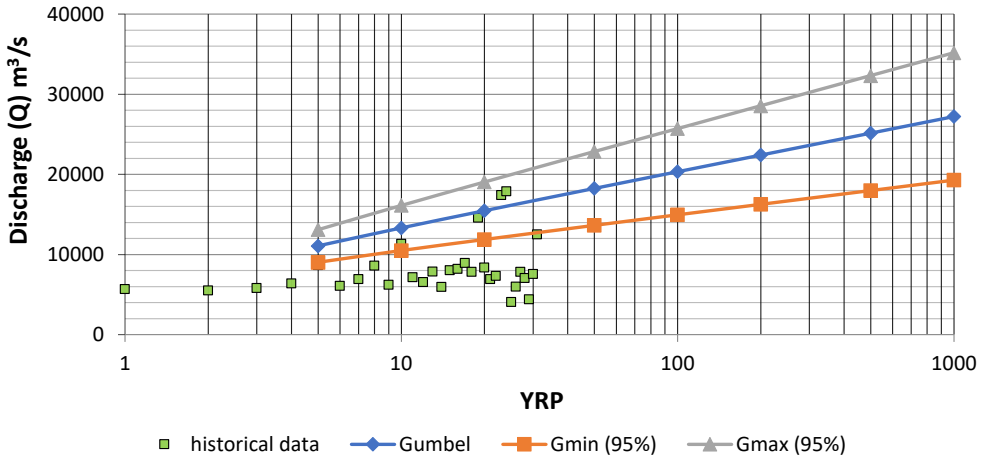

Frequency of flood discharge shows the Gumbel's Distribution and its 95% confidence limits of extreme values (calculated using the standard normal distribution). The YRP is plotted on a logarithmic scale for clarity. Historical observed discharge is also given here for reference.

Simulation of 2014 Flood Event

Flood simulation was conducted using HEC-RAS. The clipped DEM was converted into terrain in RAS-Mapper, and LULC data were imported to assign Manning's roughness coefficients for each land-cover class. Google Satellite Map and OpenStreetMap were used as background layers. The model geometry was defined by delineating the model perimeter, and a 10 m resolution computational mesh was generated. A flow hydrograph was applied as the upstream boundary condition, while normal depth was used as the downstream boundary condition. The model was calibrated using the 2009 peak discharge and validated with the 2014 peak discharge. Flood events were simulated for 36 hours with a 10-second computational interval and a 1-hour output interval. Following calibration and validation, return period flood events of the Karnali River were simulated, and flood depth and velocity outputs were exported as raster files.

Table 5

Classification of Threshold Discharge (m^3/s) Water Level Gauge Height (m) and Mean Above Sea Level (m.a.s.l.)

River	Station	Runoff (m^3/s)	Threshold by DHM water level (m)	Reference to MSL	Remarks
Karnali	Chisapani	8200	10.0	201.64	Warning level
		10,000	10.8	202.44	Danger level

Table 6

Inundate Area of Each Ward for Different YRPs

Ward	Area (km^2)				Percentage (%)			
	10-YRP	20-YRP	50-YRP	100-YRP	10-YRP	20-YRP	50-YRP	100-YRP
1	10.05	10.56	10.93	11.17	75.5	79.33	82.12	83.87
2	8.35	8.84	9.27	9.56	64.85	68.6%	71.96	74.18
3	8.90	9.42	9.81	10.09	61.26	64.86	67.5	69.44
4	5.19	5.64	5.96	6.133	62.55	67.90	71.9	73.9

Flood Hazard

Flood hazard maps for Rajapur Municipality were generated, with inundated areas quantified for 10- to 100-YRP, as shown in Figure 6 and Tables 5-6. Inundation extent increased progressively with discharge magnitude and return period, highlighting expanding high-hazard zones over time. Reference height categorized according to

the warning and danger levels for flood forecasting in Karnali used by DHM, Nepal (Gautam & Dulal, 2013)

Figure 6

Water Depth of the Karnali River in Different YRPs

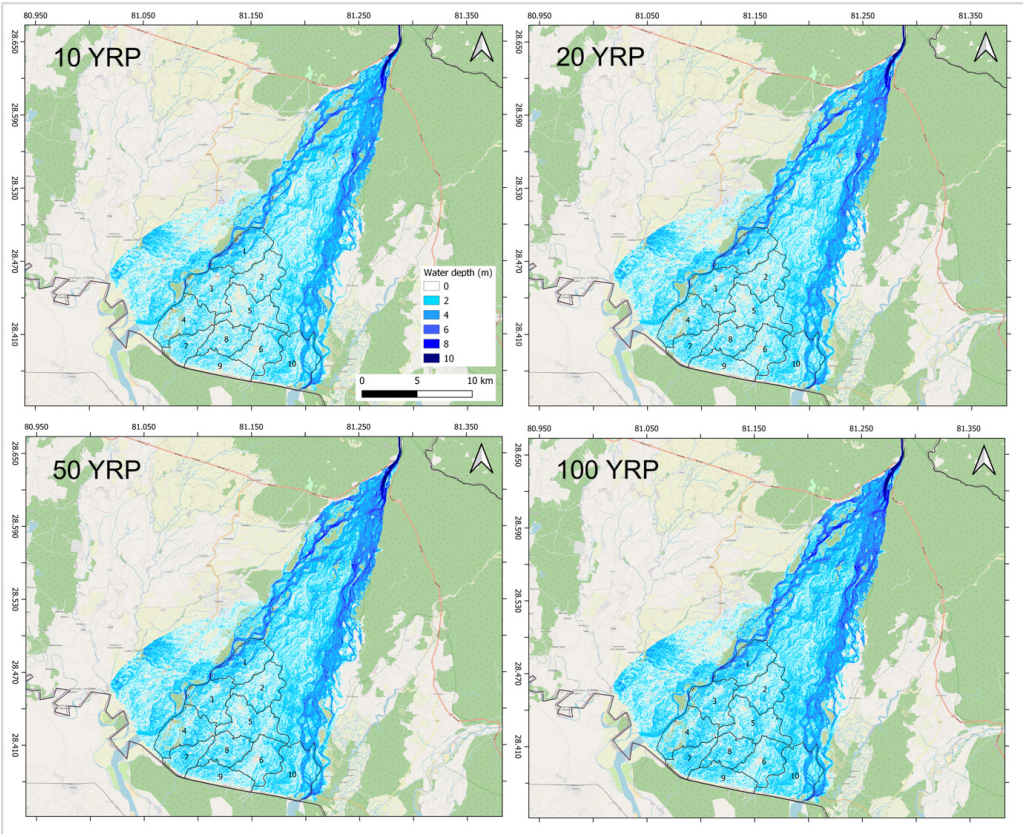

Inundation extents and depths were simulated for 10-, 20-, 50-, and 100-YRPs under progressively increasing peak discharges, with raster analysis applied to quantify affected areas (Figure 6; Tables 6–7). Ward-specific results indicated that Ward 1 was the most vulnerable, with 10.05 km² (76% of its area) inundated at the 10-YRP and 11.17 km² (84%) at the 100-YRP. All wards shows proportional increases in inundation with discharge magnitude. Depth classifications identified predominant water levels of 1–10 m across wards, which were validated against observed warning and danger thresholds during seasonal floods. Depths ≥1 m were designed as high risk due to their potential to cause severe damage.

Flood Vulnerability

Figure 7

Exposure, Sensitivity, Adaptive Capacity and Vulnerability Level of Different Wards of Rajapur Municipality

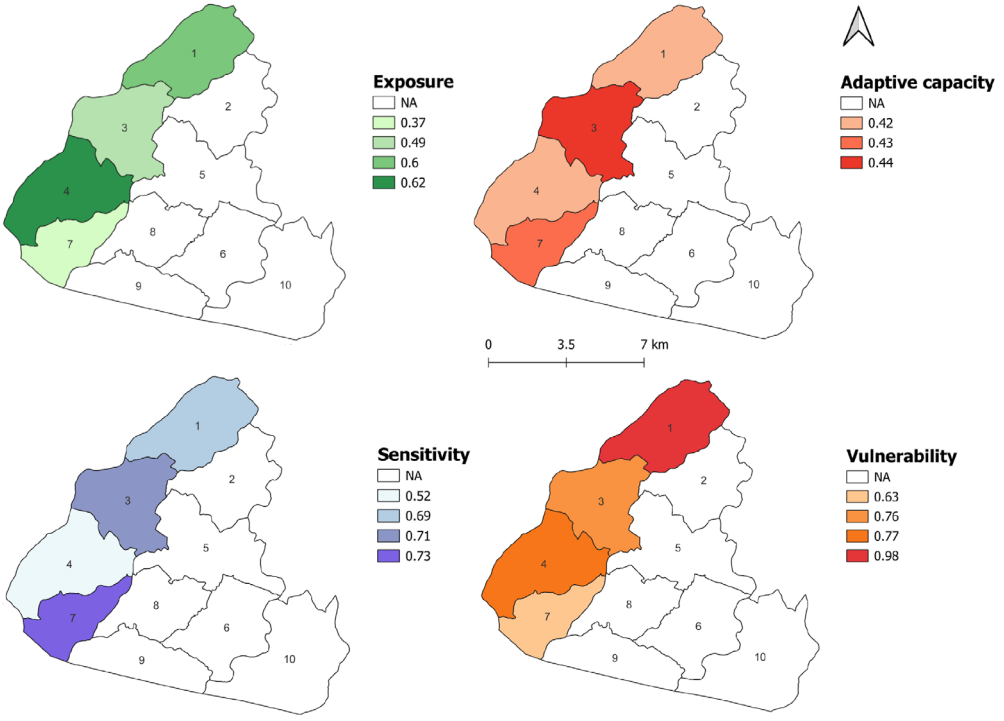

Figure 7 shows Wards 1, 3, and 4 as highly vulnerable, while Ward 7 is moderately vulnerable. Ward 1, located between the Karnali River and its Budikulo tributary, experiences converging flows, increasing its risk relative to neighboring wards. Linear settlement patterns across all four wards include substandard housing close to riverbanks (as close as 6 m), exceeding community adaptive capacities and intensifying overall vulnerability. Adjacent agricultural lands are also at risk of erosion from flood depths ≥2 m, with maximum depths reaching 10 m, as confirmed by hazard mapping, municipal reports, field observations, and vulnerability indices (Figure 7). Although some wards exhibit high exposure and sensitivity to climate-induced flooding, other show comparatively lower vulnerability due to effective adaptation strategies promoted by local government initiatives and private sector support.

Flood Risk

Risk assessments indicate that settlements across Rajapur Municipality face elevated flood and inundation hazards, intensified by the Karnali River erosion in Ward 1's

Tihuni area and persistently rising water levels. Simulations show that flood depths of upt to 10 m pose very high risk to communities and infrastructure in Wards 1, 3, 4, and 7, with all wards classified as high risk under 10-YRP conditions. Specifically, Ward 1 has 4.32 km² at very high risk within its total area of 13.32 km² (Table 6), while Wards 3, 4, and 7 exhibit substantial high-risk extents across all YRP scenarios (Table 7).

Table 7

Flood Risk Classification for Wards at Different YRPs

Ward	10-YRP (km^2)	20-YRP (km^2)	50-YRP (km^2)	100-YRP (km^2)	Risk class
Ward #1	0.73	0.003	0.282	0.46	
	0.88	0.38	0.895	0.8	
	1.02	0.99	1.12	0.99	
	3.13	3.95	1.44	2.71	
	4.32	3.99	7.22	6.25	
Ward #3	0.79	0.051	0.43	0.67	
	1.05	0.592	0.995	0.99	
	1.19	1.209	1.35	1.102	
	3.13	3.84	1.78	3.12	
	2.23	1.98	4.73	3.69	
Ward #4	1.12	0.17	0.59	0.75	
	1.24	0.75	1.12	1.08	
	1.42	1.51	1.7	1.56	
	3.44	4.15	2.16	3.73	
	1.72	1.5	4.27	3.004	
Ward #7	0.6	0.01	0.3	0.37	Very low
	0.61	0.17	0.71	0.7	Low
	0.85	0.81	0.78	0.7	Moderate
	2.11	2.71	1.04	2.04	High
	1.04	0.88	3.15	2.4	Very high

Figure 8 illustrates the flood-prone areas across various return periods in Rajapur Municipality, offering a comparative visual representation of flood risk distribution and highlighting priority areas for disaster risk reduction and climate-resilient planning.

Figure 8

Flood Risk Map of Rajapur Municipality in Different YRPs

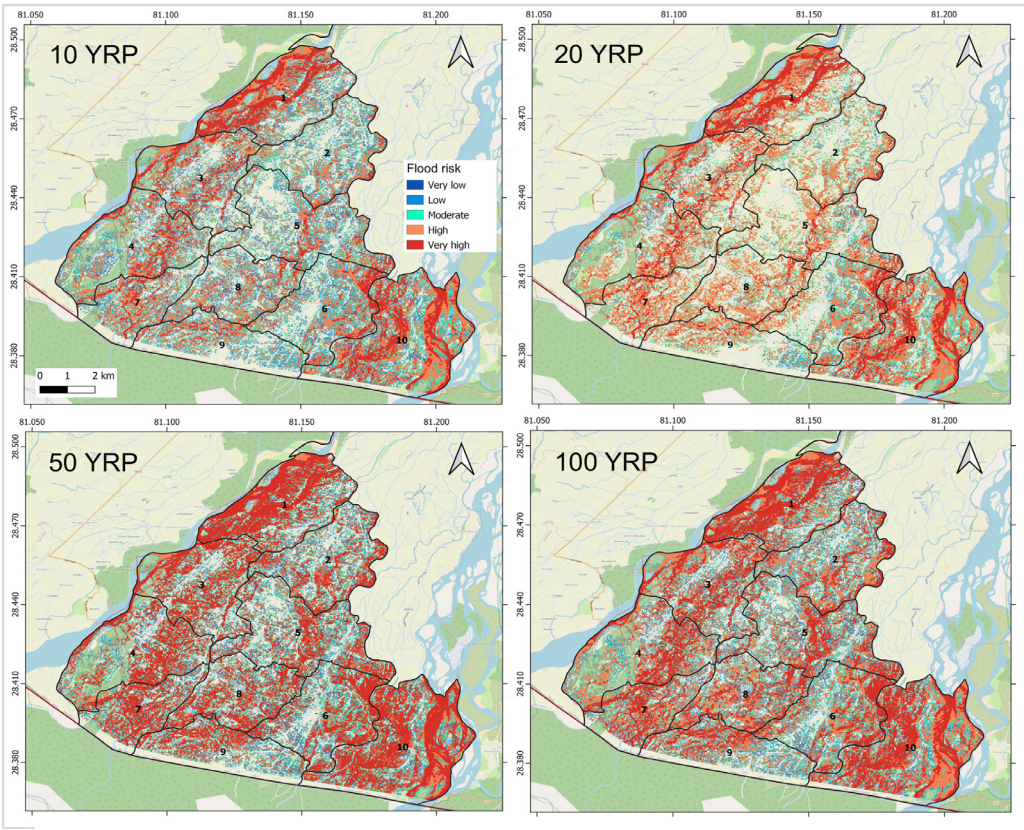

Discussion

This study applied the Type I Gumbel distribution to estimate flood frequency (Lamichhane *et al.,* 2024) and conducted hydrodynamic simulations using HEC-RAS, calibrated and validated against historical flood events (Figures 4 and 5). Results indicate that the lower reaches of the Karnali River, particularly in Wards 1, 3, 4, and 7, experience greater overflow due to increased river velocity, leading to extensive inundation. Flood depth and hazard mapping show most inundated areas fall within the 2–10 m depth class, with depths ≥1 m posing high risk to settlements, infrastructure, and agricultural lands (Figure 6; Maharjan *et al*., 2024). Ward 1 is the most vulnerable, with a substantial portion of its area at very high risk, while Wards 3, 4, and 7 also exhibit high-risk conditions under multiple return-period scenarios. These findings are consistent with prior studies highlighting the Karnali River Basin's susceptibility to

monsoon flooding and extreme discharge events (Aryal *et al*., 2020; Venkateswaran *et al*., 2015).

The findings also highlight important hydrological characteristics of lower Karnali River. In the Terai plains, distributary channel networks increase flood extent through channel shifting and overbank flow during intense monsoon events. High sediment loads further contribute to channel instability and ongoing changes in floodplain morphology. Ward-level vulnerability assessment using the Nepal VRA framework revealed that high exposure, sensitivity, and limited adaptive capacity exacerbate risks, particularly in Wards 1, 3, and 4. Ward 7, while highly sensitive, shows moderate overall vulnerability due to lower exposure, though it remains within the flood risk zone. The integration of hydraulic simulations with socioeconomic and demographic data enabled identification of critical hotspots and informed adaptation priorities at the community level. This study acknowledges limitations. Data constraints restricted finer spatial resolution, and focusing on four wards limits broader basin-scale analysis. Despite these limitations, the findings provide essential guidance for future research, including basin-wide 2D modeling, integration of climate projections, real-time monitoring, and participatory scenario planning with affected communities.

The results also highlight the need for targeted policy and planning interventions. Recommended measures include enforcing riverbank buffer zones, upgrading flood forecasting systems with real-time data, establishing multi-channel early warning systems, relocating highly vulnerable settlements, promoting climate-resilient livelihoods, and integrating vulnerability mapping into land-use planning. Collectively, these actions can enhance community resilience and reduce the adverse impacts of climate-induced flooding in Rajapur Municipality.

Conclusion

This study examines flood vulnerability in the lower KRB, where communities experience recurrent monsoon flooding that impacts livelihoods, farmland, and endangers lives due to high, sediment-laden peak flows. The findings show a clear risk across active floodplains: areas with high inundation are submerged under multiple return periods, posing serious threats to housing, infrastructure, and agriculture, while surrounding areas remain at considerable risk.

The hazard and risk maps support evidence-based floodplain management, helping to plan resilient infrastructure, regulate development in high-risk areas, and prioritize evacuation planning. The study also promotes non-structural measures, such as land-use zoning, community-based early warning systems, and riverbank awareness programs,

as cost-effective strategies to reduce loss of life and property, alongside structural flood controls.

The research emphasizes that flood resilience is not only a technical or engineering issue, but also a social priority. By translating flood susceptibility data into practical community actions, the study supports residents of dynamic floodplains in strengthening their adaptive capacity rather than remaining vulnerable to recurring monsoon floods. These findings call for integrated flood governance that combines scientific evidence with local knowledge to protect communities during monsoon seasons.

References

Aryal, D., Wang, L., Adhikari, T. R., Zhou, J., Li, X., Shrestha, M., Wang, Y., & Chen, D. (2020). A model-based flood hazard mapping on the southern slope of Himalaya. *Water (Switzerland)*, *12*. https://doi.org/10.3390/w12020540

Chyon, M. S. A., Biswas, S., Mondal, M. S., Roy, B., & Rahman, A. (2023). Integrated assessment of flood risk in Arial Khan floodplain of Bangladesh under changing climate and socioeconomic conditions. *Journal of Flood Risk Management*, *16*(2), e12876. https://doi.org/10.1111/jfr3.12876

Dangol, N. (2020). Flood modeling assessment: A case of Bishnumati River. *Journal on Geoinformatics, Nepal*, *20*(1), 31–37. https://doi.org/10.3126/njg.v20i1.39474

Dangol, S., & Bormudoi, A. (2015). Flood hazard mapping and vulnerability analysis of Bishnumati River, Nepal. *Journal on Geoinformatics*, *Nepal, 14*, 20–24. https://doi.org/10.3126/njg.v14i0.16969

Felkner, J., Tazhibayeva, K., & Townsend, R. (2009). Impact of climate change on rice production in Thailand. *American Economic Review*, *99*(2), 205–210. https://doi.org/10.1257/aer.99.2.205

Gautam, D. K., & Dulal, K. (2013). Determination of threshold runoff for flood warning in Nepalese rivers. J*ournal of Integrated Disaster Risk Management, 3*(1), 125–136. https://doi.org/10.5595/idrim.2013.0061

Hicks, F. E., & Peacock, T. (2005). Suitability of HEC-RAS for flood forecasting. *Canadian Water Resources Journal*, *30*(2), 159–174. https://doi.org/10.4296/cwrj3002159

Hisdal, H., Stahl, K., Tallaksen, L. M., & Demuth, S. (2001). Have streamflow droughts in Europe become more severe or frequent? *International Journal of Climatology*, *21*(3), 317–333. https://doi.org/10.1002/joc.619

IPCC (2014). *Climate Change 2014: Impacts, adaptation, and vulnerability. Part A: Global and Sectoral Aspects,* Cambridge University Press.

IPCC (2019). Climate change and land: An special report on climate change, desertification, land degradation, sustainable land management, food security, and greenhouse gas fluxes in terrestrial ecosystems (SR2). *Geneva, IPCC*, *650*.

Jongman, B., Ward, P. J., & Aerts, J. C. J. H. (2012). Global exposure to river and coastal flooding: Long term trends and changes. *Global Environmental Change, 22*(4), 823–835. https://doi.org/10.1016/j.gloenvcha.2012.07.004

Khatiwada, K. R., Panthi, J., Shrestha, M. L., & Nepal, S. (2016). Hydro-climatic variability in the Karnali River Basin of Nepal Himalaya. *Climate*, *4*(2), 1–14. https://doi.org/10.3390/cli4020017

Kwak, S. G., & Kim, J. H. (2017). Central limit theorem: The cornerstone of modern statistics. *Korean Journal of Anesthesiology, 70*(2), 144-156. https://doi.org/10.4097/kjae.2017.70.2.144

Lamichhane, S., Devkota, N., Poudel, H. P., & Luitel, S. (2024). Flood hazard mapping and flood vulnerability analysis of building structures at settlement-scale. *Journal of Science and Engineering*, *11*, 25–34. https://doi.org/10.3126/jsce.v11i01.73526

Maharjan, M., Timilsina, S., Ayer, S., Singh, B., Manandhar, B., & Sedhain, A. (2024). Flood susceptibility assessment using machine learning approach in the Mohana-Khutiya River of Nepal. *Natural Hazards Research, 4*(1), 32–45. https://doi.org/10.1016/j.nhres.2024.01.001

Maranzoni, A., D'Oria, M., & Rizzo, C. (2023). Quantitative flood hazard assessment methods: A review. *Journal of Flood Risk Management, 16*(1), e12855. https://doi.org/10.1111/jfr3.12855

Mohammed, K., Islam, A. K. M. S., Islam, G. M. T., Alfieri, L., Khan, Md. J. U., Bala, S. K., & Das, M. K. (2018). Future floods in Bangladesh under 1.5°C, 2°C, and 4°C global warming scenarios. *Journal of Hydrologic Engineering*, *23*(12), 04018050. https://doi.org/10.1061/(ASCE)HE.1943-5584.0001705

MoPE (2017). *Vulnerability and risk assessment framework and indicators for national adaptation plan formulation process in Nepal.* Ministry of Population and Environment (MoPE), Kathmandu

Mudashiru, R. B., Sabtu, N., Abustan, I., & Balogun, W. (2021). Flood hazard mapping methods: A review. *Journal of Hydrology, 603*, 126846. https://doi.org/10.1016/j.jhydrol.2021.126846

Pokhrel, K. P., Chidi, C., Timilsena, N. P., & Mahat, D. K. (2021). Flood hazards and livelihood challenges in lower Karnali river basin: A case from Sudur Paschim Province, Nepal. *International Journal of Innovative Science and Research Technology, 6*(5), 92-100

Poornima, R., Ramakrishnan, S., Priyatharshini, S., Poornachandhra, C., John, J. E., Ramya, A., & Dhevagi, P. (2024).Climate change implications in the Himalayas. *In:* Borthakur, A., Singh, P. (eds.) *The Himalayas in the anthropocene.* Springer, Cham. https://doi.org/10.1007/978-3-031-50101-2_11

Regmi, B. R., Sapkota, R., Paudyal, A., Gautam, D. K., Thapa, R., Joshi, R., Shah, S., G.C., G., & Mishra, B. (2023). Co-development of vulnerability and risk assessment framework and methodology for Nepal. *Environmental Monitoring and Assessment, 195*(6), 792. https://doi.org/10.1007/s10661-023-11330-6

Rentschler, J., Salhab, M., & Jafino, B. A. (2022). Flood exposure and poverty in 188 countries. *Nature Communications*, *13*(1), 3527. https://doi.org/10.1038/s41467-022-30727-4

Rusk, J., Maharjan, A., Tiwari, P., Chen, T.-H. K., Shneiderman, S., Turin, M., & Seto, K. C. (2022). Multi-hazard susceptibility and exposure assessment of the Hindu Kush Himalaya. *Science of The Total Environment*, *804*, 150039. https://doi.org/10.1016/j.scitotenv.2021.150039

Singh, M., Thomas, A., Khalko, V., & Kumar, V. (2020). Flood hazard mapping using HEC-RAS and QGIS for Meja dam. *International Journal of Chemical Studies, 8*(5), 2044–2047. https://doi.org/10.22271/chemi.2020.v8.i5ab.10604

Steiniger, S., & Hunter, A. J. S. (2013). The 2012 free and open source GIS software map – A guide to facilitate research, development, and adoption. *Computers, Environment and Urban Systems, 39,* 136–150. https://doi.org/10.1016/j.compenvurbsys.2012.10.003

Thakuri, S., Dahal, S., Shrestha, D., Guyennon, N., Romano, E., Colombo, N., & Salerno, F. (2019). Elevation-dependent warming of maximum air temperature in Nepal during 1976–2015. *Atmospheric Research*, *228*, 261-269. https://doi.org/10.1016/j.atmosres.2019.06.006.

Vashishtha, D. & Fazal, S. (2025). An appraisal of livelihood sustainability and climate change vulnerability in Uttar Pradesh: Emerging trends and impacts. *In:* N. Banu & S. Fazal (eds.), *Livelihoods and well-being in the era of climate change*. Springer Nature Switzerland, pp. 261–286. https://doi.org/10.1007/978-3-031-81132-6_13

Vashist, K., & Singh, K. K. (2023). HEC-RAS 2D modeling for flood inundation mapping: A case study of the Krishna River Basin. *Water Practice & Technology, 18*(4), 831–844. https://doi.org/10.2166/wpt.2023.048

Venkateswaran, K., MacClune, K., Dixit, K. M., Yadav, S., Maharjan, R., & Dugar, S. (2015). *Risk nexus: Urgent case for recovery—What we can learn from the August 2014 Karnali River floods in Nepal*. ISET-International & ISET-Nepal.

Winsemius, H. C., Van Beek, L. P. H., Jongman, B., Ward, P. J., & Bouwman, A. (2013). A framework for global river flood risk assessments. *Hydrology and Earth System Sciences, 17*(5), 1871–1892. https://doi.org/10.5194/hess-17-1871-2013

Zelenhasic, E. F. (1970). *Theoretical probability distributions for flood peaks*. *hydrology paper 42*. Colorado State University (Fort Collins).

Žurovec, O., Čadro, S., & Sitaula, B. (2017). Quantitative assessment of vulnerability to climate change in rural municipalities of Bosnia and Herzegovina. *Sustainability*, *9*(7), 1208. https://doi.org/10.3390/su9071208